Supporting Information

Copper interface promotes the transformation of nickel hydroxide into high-valent nickel for efficient oxygen evolution reaction

Junjun Zhang,[a] Fengchen Zhou,[b] Aiming Huang,[b] Yong Wang,[b] Wei Chu,*[a] Wen Luo*[b]

[a] Department of Chemical Engineering, Sichuan University, Chengdu 610065, China
[b] School of Environmental and Chemical Engineering, Shanghai University, 99 Shangda Road, Shanghai 200444, China

Corresponding author: chuwei1965@foxmail.com; wenluo@shu.edu.cn

1. Experimental section

1.1 Preparation of electrodes

Figure 1 shows the schematic illustration of the synthesis of the $Ni(OH)_2$/Cu/NF catalyst. Specifically, a 1x1 cm^2 NF was soaked in dilute hydrochloric acid solution for 3 min and then rinsed with ultrapure water. Next, it was soaked in acetone solution for 15 min followed by washing with ultrapure water to remove impurities from the surface. For the electrodeposition of Cu/NF, a Chronoamperometry method was used with Ag/AgCl as the reference electrode, graphite rod as the counter electrode, and NF as the working electrode. The NF was immersed in 50 mL of deposition solution containing 0.10 $mol·L^{-1}$ $CuSO_4·5H_2O$ and 0.40 $mol·L^{-1}$ H_3BO_3. The deposition potential was -0.90 V, and the deposition time was 30 min. The Cu/NF electrode prepared in the last step was used as the working electrode and immersed in a 50 mL deposition solution containing 0.10 $mol·L^{-1}$ $Ni(NO_3)_2·6H_2O$ for electrodeposition to obtain the $Ni(OH)_2$/Cu/NF electrode. The preparation method of $Ni(OH)_2$/NF electrode is similar to the above steps, except that there is no electrodeposited Cu. In addition, the spent $Ni(OH)_2$/NF and $Ni(OH)_2$/Cu/NF electrodes mentioned in the article were obtained by reacting at a current density of 100 $mA·cm^{-2}$ for 12 hours after OER.

1.2 Characterization

The microscopic morphology, crystal structure and composition of the catalyst were obtained by using scanning electron microscopy (SEM, ZEISS Sigma 300), transmission electron microscopy (JEOL JEM 2100F), X-ray diffraction (D8 Advance), and in situ Raman spectroscopy (Renishaw invia).

1.3 Electrochemical Measurements

All electrochemical tests in this study were performed in a 1.0 $mol·L^{-1}$ KOH electrolyte using a three-electrode system at an electrochemical workstation (CHI760E). The working, reference, and counter electrodes used were the as-prepared electrodes, Ag/AgCl, and carbon rods, respectively. The area of the immersed working electrode is 0.5 cm×1.0 cm. When calculating the current density, we considered the area of both sides of the electrodes, that is 1 cm^2. The measured potential was converted to the standard reference hydrogen electrode using the formula: E(RHE) = E(Ag/AgCl) + 0.197 + 0.059×pH. All potentials were ohmic-corrected. The specific setting parameters during electrochemical testing are described in the OER performance test chapter.
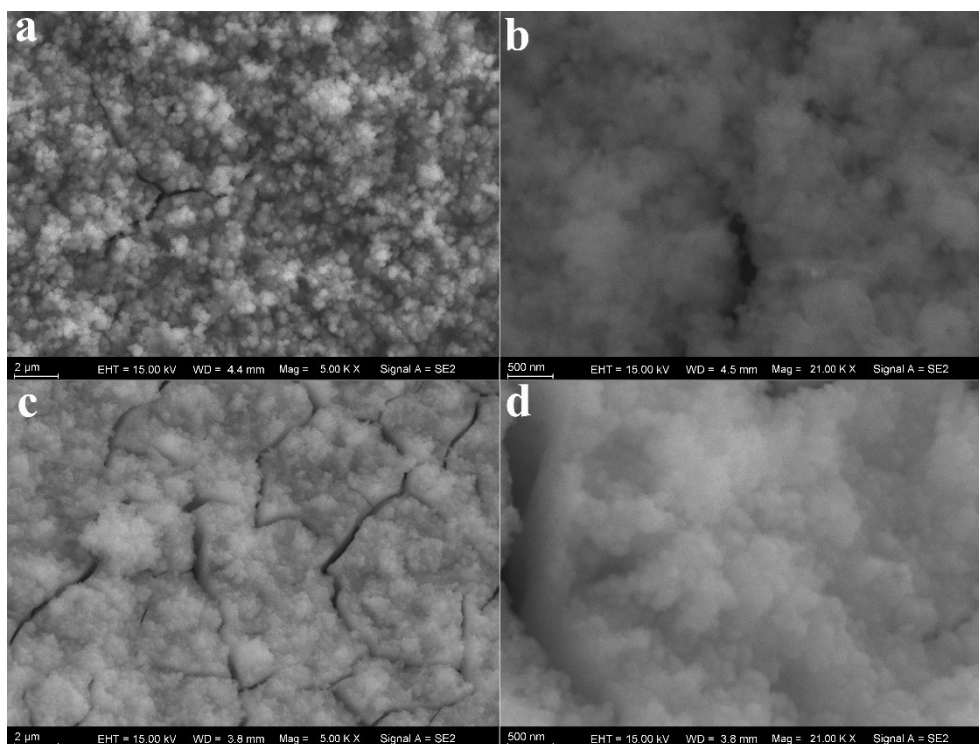
Figure S1 SEM images of Ni(OH)$_2$/NF (after OER) (a, b) ; Ni(OH)$_2$/Cu/NF (after OER) (c, d).
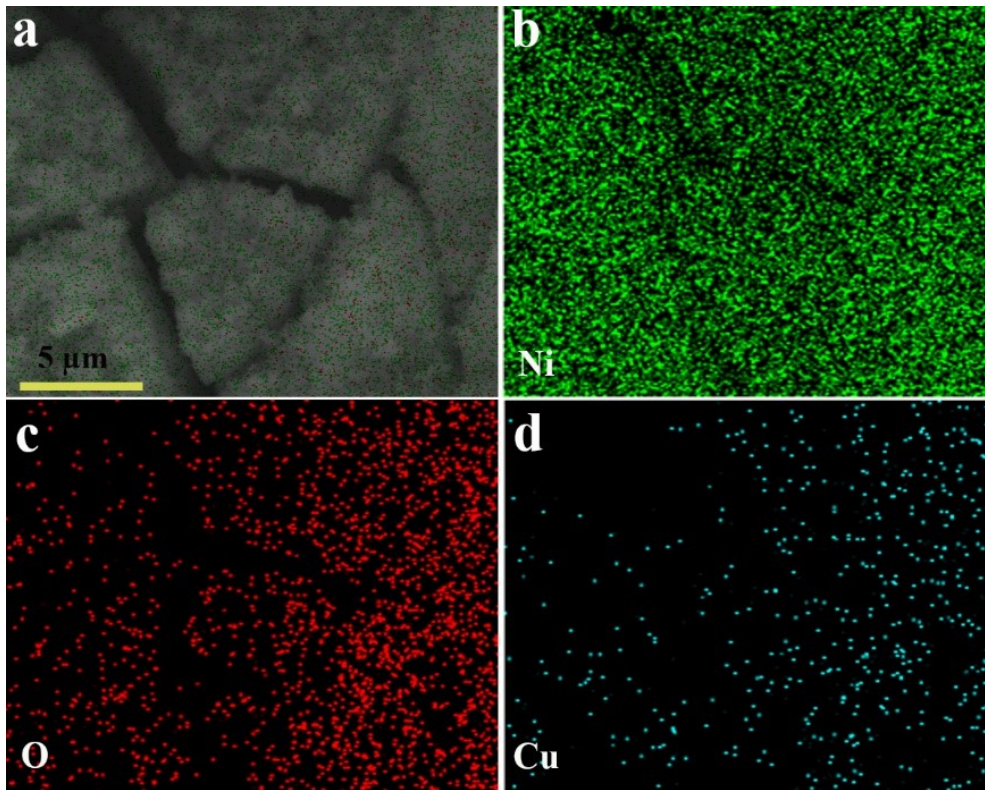
Figure S2. EDS maps of the Ni(OH)$_2$/Cu/NF , corresponding to the distribution of Ni, Cu and O elements, respectively.
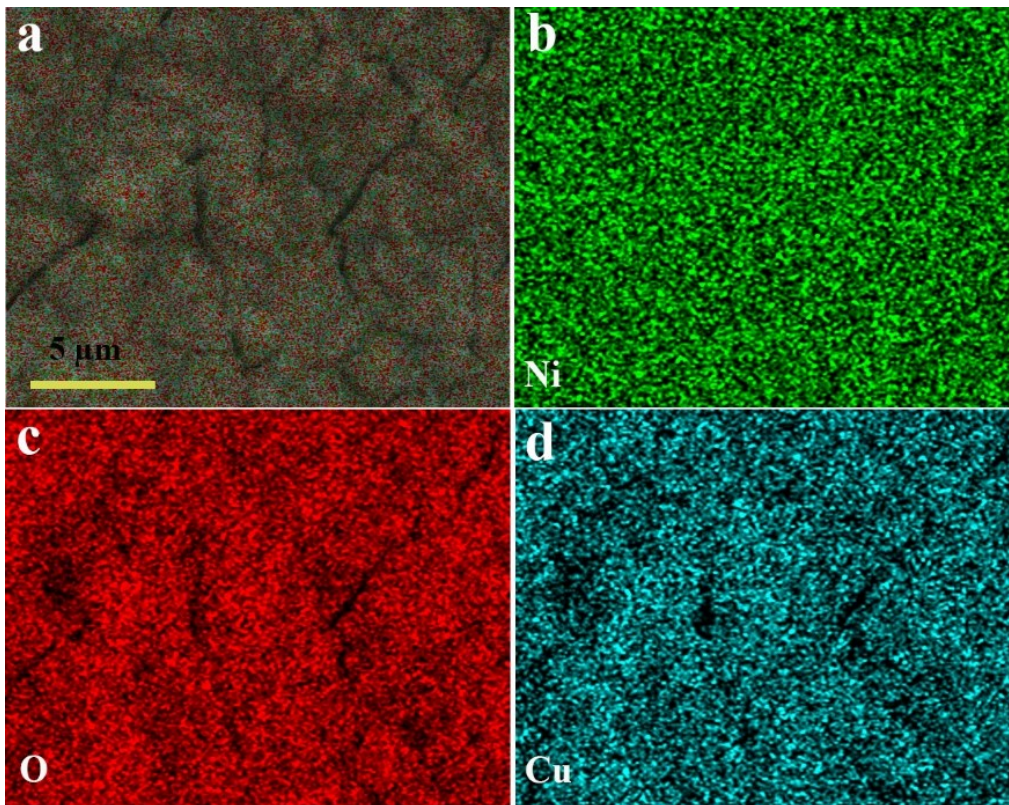
Figure S3. EDS maps of the Ni(OH)$_2$/Cu/NF (after OER) , corresponding to the distribution of Ni, Cu and O elements, respectively.
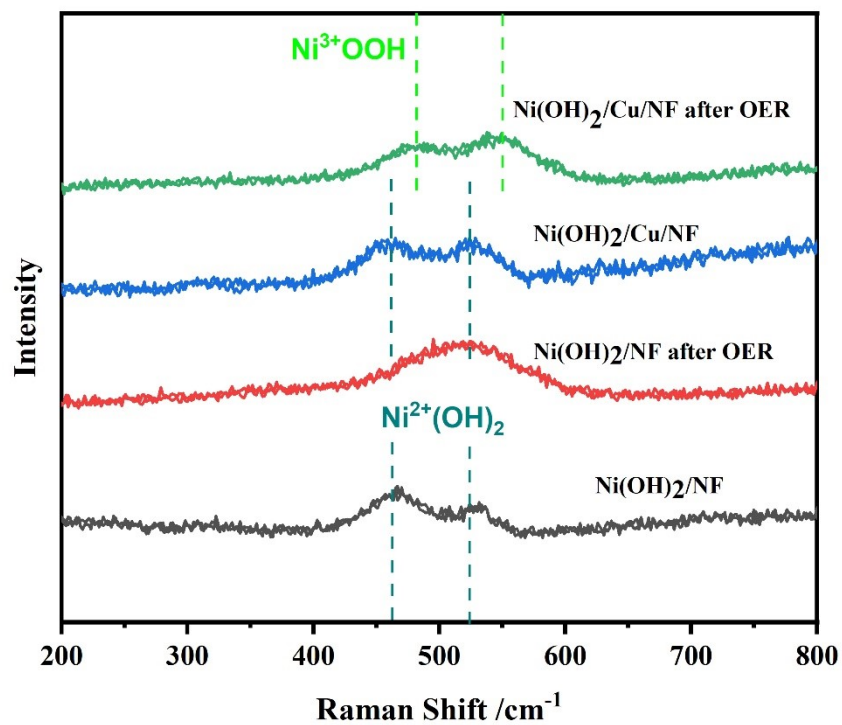
Figure S4. Ex-situ Raman spectroscopy of the Ni(OH)$_2$/NF , Ni(OH)$_2$/NF (after OER), Ni(OH)$_2$/Cu/NF, Ni(OH)$_2$/Cu/NF (after OER).
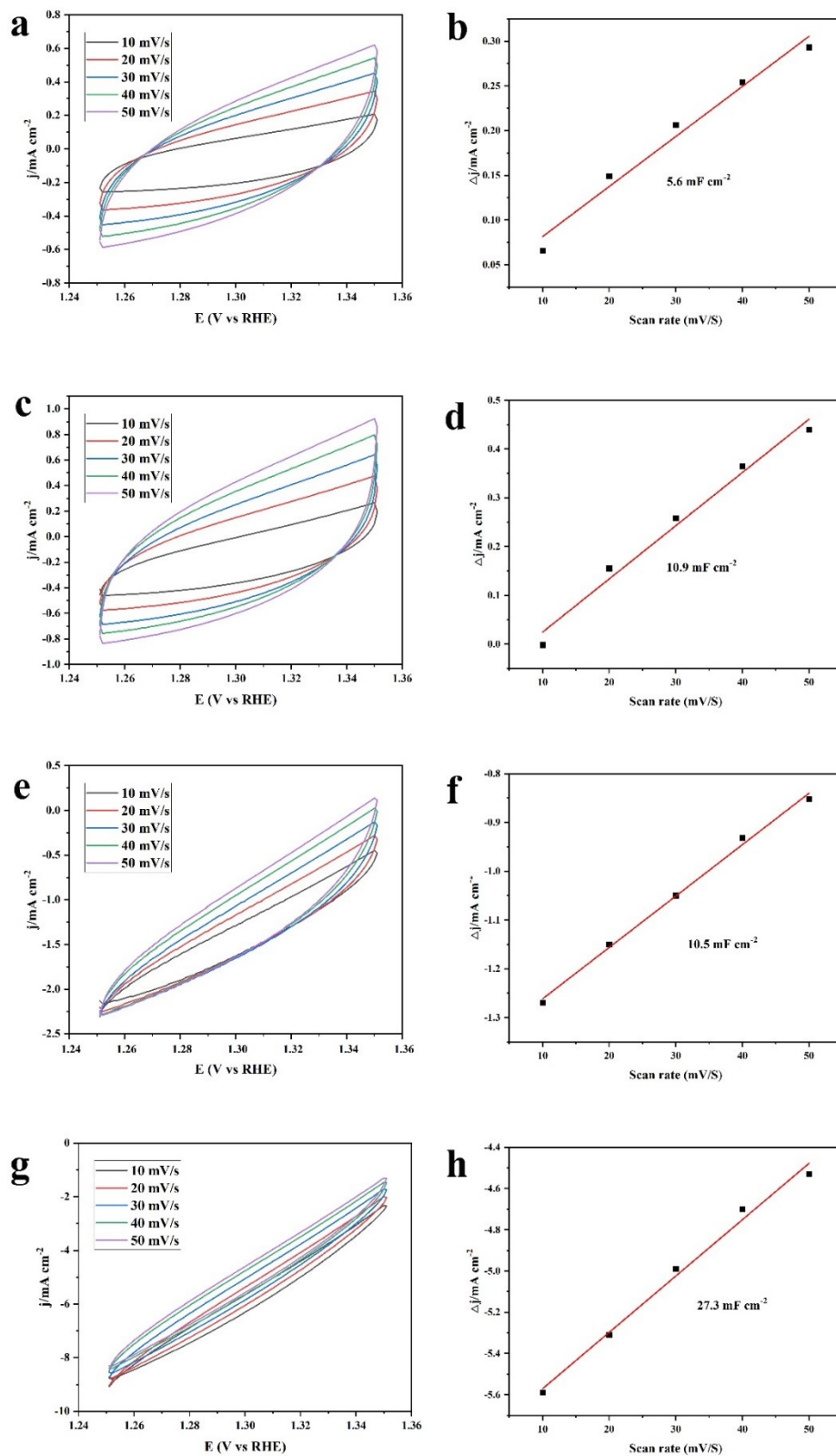
Figure S5. CV plot of NF (a), Cu/NF (c), Ni(OH)$_2$/NF (e), Ni(OH)$_2$/Cu/NF (g) at different scan rate; Double-layer capacitance for different electrodes, NF (b), Cu/NF (d), Ni(OH)$_2$/NF (f), Ni(OH)$_2$/Cu/NF (h).
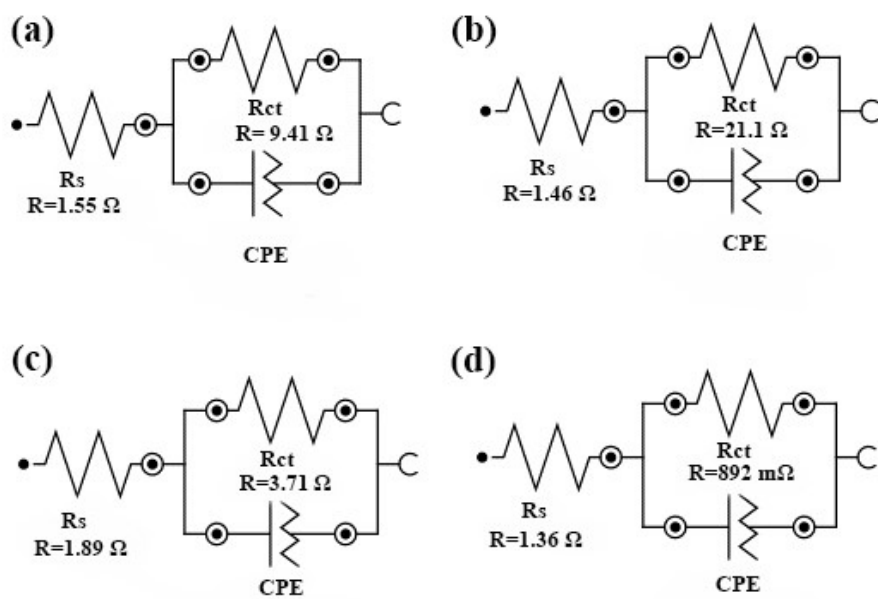
Figure S6. Impedance fitting circuit diagram of NF (a), Cu/NF (b), Ni(OH)$_2$/NF (c), Ni(OH)$_2$/Cu/NF (d).

Table S1 Impedance fitting results for different electrodes.

Electrode	Solution resistance (Rs, Ω)	Charge transfer resistance （Rct, Ω）
NF	1.55	9.41
Cu/NF	1.46	21.1
Ni(OH)$_2$/NF	1.89	3.71
Ni(OH)$_2$/Cu/NF	1.36	0.892

Table S2 Comparison of OER performance of the Ni(OH)$_2$/Cu/NF with some reported excellent Ni-based catalysts.

Catalysts	Electrolyte	Overpotential at 100 mA cm^{-2} (mV)	Tafel slope (mV dec^{-1})	Ref.
FCN-BTCMOF	1 M KOH	250	29.3	[1]
FeNi-HDNAs	1 M KOH	300	91.66	[2]
NiFeB	1 M KOH	252	-	[3]
LaNi5	1 M KOH	322	59	[4]
NiFe LDH-PANI	1 M KOH	270	44	[5]
FeCoNiMnRu/CNFs	1 M KOH	308	61.3	[6]
NiTe$_2$/NF@CuFe	1 M KOH	265	33	[7]
NiCoP/CC	1 M KOH	330	64.2	[8]
Ni$_2$S	1 M KOH	348	59	[9]
MoFe:Ni(OH)$_2$/NiOOH	1 M KOH	280	47	[10]
S/N-CMF@Fe$_x$Co$_y$Ni$_{1-x-y-}$MOF	1 M KOH	About 320	53.5	[11]
a-NiCo/NC	1 M KOH	About 300	49	[12]
Fe–Ni(O)OH	1 M KOH	289	48	[13]
NiFeW3-LDHs	1 M KOH	256	36.44	[14]
Ni$_5$P$_4$@FeP	1 M KOH	242	43.93	[15]
Ni(OH)$_2$/Cu/NF	1 M KOH	260	41	This work

References

[1] Li Z, Deng S, Yu H, et al. Fe–Co–Ni trimetallic organic framework chrysanthemum-like nanoflowers: efficient and durable oxygen evolution electrocatalysts [J]. Journal of Materials Chemistry A, 2022, 10(8): 4230-4241.

[2] Yu N, Cao W, Huttula M, et al. Fabrication of FeNi hydroxides double-shell nanotube arrays with enhanced performance for oxygen evolution reaction [J]. Applied Catalysis B: Environmental, 2020, 261.

[3] Bai Y, Wu Y, Zhou X, et al. Promoting nickel oxidation state transitions in single-layer NiFeB hydroxide nanosheets for efficient oxygen evolution [J]. Nat Commun, 2022, 13(1): 6094.

[4] Chen Z, Yang H, Mebs S, et al. Reviving Oxygen Evolution Electrocatalysis of Bulk La-Ni Intermetallics via Gaseous Hydrogen Engineering [J]. Adv Mater, 2022: e2208337.

[5] Zhang J, Zhang H, Huang Y. Electron-rich NiFe layered double hydroxides via interface engineering for boosting electrocatalytic oxygen evolution [J]. Applied Catalysis B: Environmental, 2021, 297.

[6] Hao J, Zhuang Z, Cao K, et al. Unraveling the electronegativity-dominated intermediate adsorption on high-entropy alloy electrocatalysts [J]. Nat Commun, 2022, 13(1): 2662.

[7] Jin Z, Zheng H, Dong Y, et al. Effect of Interfacial Strength and Anchoring in a Highly Efficient $NiTe_2$/NF@CuFe Oxygen-Evolution Catalyst [J]. ACS Sustainable Chemistry & Engineering, 2022, 10(46): 15166-15174.

[8] Du C, Yang L, Yang F, et al. Nest-like NiCoP for Highly Efficient Overall Water Splitting [J]. ACS Catalysis, 2017, 7(6): 4131-4137.

[9] Mondal I, Hausmann J N, Vijaykumar G, et al. Nanostructured Intermetallic Nickel Silicide (Pre)Catalyst for Anodic Oxygen Evolution Reaction and Selective Dehydrogenation of Primary Amines [J]. Advanced Energy Materials, 2022, 12(25).

[10] Jin Y, Huang S, Yue X, et al. Mo- and Fe-Modified $Ni(OH)_2$/NiOOH Nanosheets as Highly Active and Stable Electrocatalysts for Oxygen Evolution Reaction [J]. ACS Catalysis, 2018, 8(3): 2359-2363.

[11] Zhao Y, Lu X F, Wu Z P, et al. Supporting Trimetallic Metal-Organic Frameworks on S/N-Doped Carbon Macroporous Fibers for Highly Efficient Electrocatalytic Oxygen Evolution [J]. Adv Mater, 2023, 35(19): e2207888.

[12]Pei Z, Lu X F, Zhang H, et al. Highly Efficient Electrocatalytic Oxygen Evolution Over Atomically Dispersed Synergistic Ni/Co Dual Sites [J]. Angew Chem Int Ed Engl, 2022, 61(40): e202207537.

[13]Hua W, Sun H, Jiang M, et al. Cascading reconstruction to induce highly disordered Fe–Ni(O)OH toward enhanced oxygen evolution reaction [J]. Journal of Materials Chemistry A, 2022, 10(13): 7366-7372.

[14]Li H, Zhang C, Xiang W, et al. Efficient electrocatalysis for oxygen evolution: W-doped NiFe nanosheets with oxygen vacancies constructed by facile electrodeposition and corrosion [J]. Chemical Engineering Journal, 2023, 452.

[15]Li Y, Wu Y, Hao H, et al. In situ unraveling surface reconstruction of Ni_5P_4@FeP nanosheet array for superior alkaline oxygen evolution reaction [J]. Applied Catalysis B: Environmental, 2022, 305.